Supporting Information: Proton-Selective ^{17}O–^{1}H Distance Measurements in Fast Magic-Angle-Spinning Solid-State NMR Spectroscopy for the Determination of Hydrogen Bond Lengths

Andreas Brinkmann*, and Arno P. M. Kentgens

Physical Chemistry / Solid State NMR, Institute for Molecules and Materials, Radboud University Nijmegen, Toernooiveld 1, 6525 ED Nijmegen, The Netherlands.
*E-mail: A.Brinkmann@science.ru.nl

1 The SR4$_1^2$ Pulse Sequence

The SR4$_1^2$ pulse sequence supercycle is constructed from the basic rotor-synchronized sequence R$_1^2$ employing a single 180_0 pulse as basic element, where the notation β_ϕ denotes an rf pulse of flip angle β and phase ϕ (both in degrees):

$$\mathrm{R4}_1^2 = 180_{90}\,180_{-90}\,180_{90}\,180_{-90} \tag{S1}$$

$$= 180_{90}\,180_{270}\,180_{90}\,180_{270}, \tag{S2}$$

The basic R4$_1^2$ sequence spans exactly one rotational period. The general properties of symmetry based recoupling sequences denoted RN_n^ν and possible supercycling schemes have been discussed in great detail in Refs. 1–8. The SR4$_1^2$ supercycle is constructed in two steps from the basic sequence R4$_1^2$: (i) An inversion supercycle is formed by adding a consecutive block

$$\mathrm{R4}_1^{-2} = 180_{-90}\,180_{90}\,180_{-90}\,180_{90} \tag{S3}$$

$$= 180_{270}\,180_{90}\,180_{270}\,180_{90}. \tag{S4}$$

(ii) The combined block R4$_1^2$R4$_1^{-2}$ is subjected to a 3 step "multiple-quantum" (MQ) phase cycle, in which the overall rf phase of consecutive pulse sequence blocks is incremented in

steps of 120°.[3,8–11] The nested supercycle $(\mathrm{R4}_1^2\mathrm{R4}_1^{-2})3^1$ is denoted $\mathrm{SR4}_1^2$ and is given by

$$\begin{aligned}
\mathrm{SR4}_1^2 &= (\mathrm{R4}_1^2\mathrm{R4}_1^{-2})3^1 && \text{(S5)}\\
&= \left[\mathrm{R4}_1^2\mathrm{R4}_1^{-2}\right]_0 \left[\mathrm{R4}_1^2\mathrm{R4}_1^{-2}\right]_{120} \left[\mathrm{R4}_1^2\mathrm{R4}_1^{-2}\right]_{240} && \text{(S6)}\\
&= 180_{90}\ \ 180_{270}\ 180_{90}\ \ 180_{270}\ \ 180_{270}\ 180_{90}\ \ 180_{270}\ 180_{90} && \text{(S7)}\\
&\quad\ 180_{210}\ 180_{30}\ \ 180_{210}\ 180_{30}\ \ \ 180_{30}\ \ 180_{210}\ 180_{30}\ \ 180_{210}\\
&\quad\ 180_{330}\ 180_{150}\ 180_{330}\ 180_{150}\ \ 180_{150}\ 180_{330}\ 180_{150}\ 180_{330},
\end{aligned}$$

where a single 180_0 pulse is assumed as basic element. As a consequence the $\mathrm{SR4}_1^2$ sequence requires the rf field strength to be twice the spinning frequency. Other possible choices for the basic element, especially for application at lower spinning frequencies, are composite pulses[12] (e. g. $90_{180}270_0$) or windowed elements.[13]

Consider a spin system consisting of a single half-integer quadrupolar S-spin and several spin-1/2 I-spins. The $\mathrm{SR4}_1^2$ sequence is solely applied to the I-spins. It achieves longitudinal two-spin-order (I_zS_z) recoupling of the IS heteronuclear dipolar couplings while decoupling the homonuclear I-spin dipolar interactions. In detail, the sequence $\mathrm{SR4}_1^2$ has the same properties as the heteronuclear longitudinal two-spin-order recoupling sequences $(\mathrm{R32}_8^{15}\mathrm{R32}_8^{-15})2^1$ and $(\mathrm{R32}_8^{15}\mathrm{R32}_8^{-15})3^1$, recently presented,[14] namely: (i) Heteronuclear dipolar coupling terms proportional to I_zS_z are recoupled in the first order average Hamiltonian. (ii) The recoupled terms of the IS heteronuclear dipolar interactions commute for different spin pairs. Hence dipolar truncation is absent. (iii) I-spin CSA terms proportional to I_z are recoupled. These terms commute with the heteronuclear dipolar coupling terms. As a consequence the oscillations of the S-spin signal due to the heteronuclear dipolar couplings are not sensitive to the I-spin chemical shift anisotropies. (iv) The I-spin homonuclear isotropic J-couplings are present under any $\mathrm{R}N_n^\nu$ sequence on the I-spins. However, in the cases considered here these couplings are very small and have no influence on the S-spin evolution. (v) All terms of the homonuclear dipolar couplings between I-spins, isotropic chemical shifts of the I-spins and isotropic heteronuclear J-couplings between S- and I-spins are suppressed in the first-order average Hamiltonian.

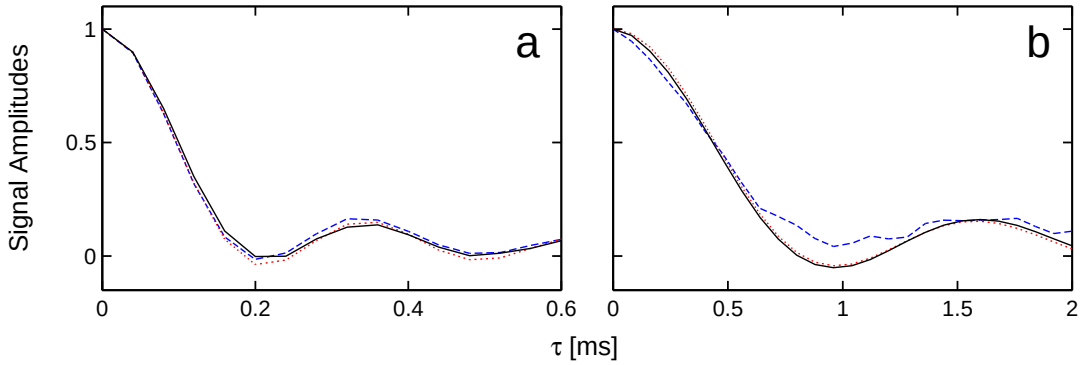

Figure S1: Normalized simulated ^{17}O signal amplitudes for the pulse sequence in Figure 2b employing different heteronuclear recoupling sequences of duration τ in an external field of 18.1 T and at a spinning frequency of 50 kHz in $^{17}O^{\eta}$-L-tyrosine·HCl, where the $^{17}O^{\eta}$–$^{1}H^{\eta}$ and $^{17}O^{\eta}\cdots{}^{1}H''$ dipolar coupling constants were set to 14200 and 3100 Hz, respectively. In addition, the numerical simulations took the spin interactions given in section 2.3 into account. (a) Employing a $^{1}H^{\eta}$-selective Gaussian pulse (dipolar oscillations due to the $^{17}O^{\eta}$–$^{1}H^{\eta}$ dipolar coupling): Solid line: Numerical three-spin ($^{17}O^{\eta}$, $^{1}H^{\eta}$, $^{1}H''$) simulations for the sequence $SR4_1^2$. Dashed line: Numerical three-spin simulations for the sequence $(R32_8^{15}R32_8^{-15})3^1$. Dotted line: Two-spin ($^{17}O^{\eta}$, $^{1}H^{\eta}$) average Hamiltonian calculations.[14] (b) Employing a $^{1}H''$-selective Gaussian pulse (dipolar oscillations due to the $^{17}O^{\eta}\cdots{}^{1}H''$ dipolar coupling): Solid line: Numerical three-spin simulations for the sequence $SR4_1^2$. Dashed line: Numerical three-spin simulations for the sequence $(R32_8^{15}R32_8^{-15})3^1$. Dotted line: Two-spin ($^{17}O^{\eta}$, $^{1}H''$) average Hamiltonian calculations.[14]

It should be noted that the plain sequence $R4_1^2$ (without supercycling) *does not* possess the same properties as the plain sequence $R32_8^{15}$. As the phase shift between consecutive 180° pulses in the $SR4_1^2$ sequence is given by 180°, adjacent pairs of 180° pulses combine to achieve an internal compensation for rf field errors.[4]

Figure S1 shows the results of numerically exact spin simulations to demonstrate the essentially improved performance of the $SR4_1^2$ sequence compared to the $(R32_8^{15}R32_8^{-15})3^1$ sequence. For the short-range $^{17}O^{\eta}$–$^{1}H^{\eta}$ interbond distance (Figure S1a) numerical three-spin simulations for both recoupling sequences agree very well with average Hamiltonian two-spin calculations that solely take the $^{17}O^{\eta}$–$^{1}H^{\eta}$ heteronuclear dipolar coupling into account. However, for the medium-range $^{17}O^{\eta}\cdots{}^{1}H''$ intermolecular distance (Figure S1b) only the numerical simulations for the $SR4_1^2$ sequence agree very well with average Hamiltonian calculations solely considering the $^{17}O^{\eta}\cdots{}^{1}H''$ dipolar coupling, whereas the numerical simulations for the $(R32_8^{15}R32_8^{-15})3^1$ sequence shows relatively large deviations.

2 Details of the Experiments and Simulations

2.1 Sample

[35–40 %-$^{17}O^{\eta}$]-L-tyrosine was purchased from Cambridge Isotope Laboratories and recrystallized from a 9 M solution of HCl in water by slow evaporation of the solvent at room temperature.

2.2 Solid-state NMR

All experiments were performed at static magnetic fields of 18.8 T and a spinning frequency of 50 kHz using a Varian Infinity+ console and a homebuilt double-resonance MAS probehead utilizing a Samoson 1.8 mm stator.[15] Zirconia rotors with a restricted sample volume of 5.3 μl were used for all experiments. Processing of the NMR data was done using the matNMR[16] processing package.

For all experiments a convergent DFS was used with starting and finishing frequencies of 1.4 MHz and 100 kHz, respectively. The ^{17}O rf field strength and sweep duration were set to 17 kHz and 2 ms respectively. The duration of the ^{17}O central-transition selective 90° and 180° pulses were given by 11 μs and 20 μs (one rotational period), respectively. The ^{1}H rf field strength during the $SR4_1^2$ heteronuclear recoupling sequence was set to 100 kHz. To verify the exact setting of the rf field strength a complete proton two-dimensional (2D) nutation spectrum was acquired. In the case of the non-proton-selective experiment (Figure 2a) low-power continuous-wave (CW) proton decoupling with a ^{1}H rf field strength of about 5 kHz was applied during the time interval $T - \tau$ and signal acquisition. In case of the proton-selective experiment (Figure 2b), CW proton decoupling with a rf field strength of about 5 kHz was applied during signal acquisition. The duration of the Gaussian pulse in the proton-selective experiment was set to 51 rotational periods (1.02 ms) and the frequency offset and rf amplitude was optimized to selectively invert $^{1}H^{\eta}$ and $^{1}H''$ longitudinal magnetization respectively, as shown in Figures 3c and 3e.

In the case of the non-proton-selective experiment (pulse scheme Figure 2a) the fol-

lowing phase-cycling scheme was employed for the rf phases Φ_{90} and Φ_{180} of the ^{17}O central-transition 90° and 180° pulses, respectively, and the post-digitization phase shift Φ_{dig}:[17]

$$\Phi_{90} = (0°)^4, (90°)^4, (180°)^4, (270°)^4 \tag{S8}$$

$$\Phi_{180} = (0°, 90°, 180°, 270°)^4 \tag{S9}$$

$$\Phi_{\text{dig}} = (0°, 180°)^2, (270°, 90°)^2, (180°, 0°)^2, (90°, 270°)^2, \tag{S10}$$

where the superscripts indicate the number of repetitions of the bracketed phase shifts.

In the case of the proton-selective experiment (pulse scheme Figure 2b), in addition, the phase-cycling included the rf phase Φ_{G} of the Gaussian pulse on the protons:

$$\Phi_{90} = \left[(0°)^4, (90°)^4, (180°)^4, (270°)^4\right]^4 \tag{S11}$$

$$\Phi_{180} = \left[(0°, 90°, 180°, 270°)^4\right]^4 \tag{S12}$$

$$\Phi_{\text{G}} = (0°)^{16}, (90°)^{16}, (180°)^{16}, (270°)^{16} \tag{S13}$$

$$\Phi_{\text{dig}} = \left[(0°, 180°)^2, (270°, 90°)^2, (180°, 0°)^2, (90°, 270°)^2\right]^4. \tag{S14}$$

2.3 Numerical Simulations

Numerically exact spin simulations were performed using SIMPSON.[18] Let $\Omega_{MR} = \{\alpha_{MR}, \beta_{MR}, \gamma_{MR}\}$ denote the Euler angles describing the relative orientation of the molecular axis system and the rotor-fixed frame. For the two-spin simulations powder averaging was accomplished using a set of 986 pairs of $\{\alpha_{MR}, \beta_{MR}\}$ angles chosen according to the ZCW scheme[19] together with stepping the γ_{MR} angle equally from 0° to 360° in 31 steps. For the three-spin simulations 376 pairs of $\{\alpha_{MR}, \beta_{MR}\}$ ZCW angles together with 19 steps in the γ_{MR} angle were used. All spin interactions of the nuclei of interest listed in Table S1 were included in the simulations.[14] The first- and second-order quadrupolar coupling was included in the simulations, whereas the second-order cross term between the quadrupolar coupling and the heteronuclear ^{17}O–^{1}H dipolar coupling was ignored, since the size of this

Quadrupole Coupling

Nucleus	C_{Q} [MHz]	η_{Q}	Ω_{PM}^{Q} [°]^a
$^{17}\mathrm{O}^{\eta}$	8.52^b	0.74^b	$\{-99, 45, 89\}^c$

Chemical Shifts

Nucleus	δ_{iso} [ppm]	δ_{aniso} [ppm]	η	$\Omega_{PM}^{\mathrm{CSA}}$ [°]^a
$^{17}\mathrm{O}^{\eta}$	43.7^d	46.5^c	0.70^c	$\{-96, 28, -80\}^c$
$^{1}\mathrm{H}^{\eta}$	0.0^d	-23.9^c	0.43^c	$\{-72, 169, -77\}^c$
$^{1}\mathrm{H}''$	2.5^d	-18.6^c	0.35^c	$\{71, 120, 55\}^c$

[a] The Euler angles Ω_{PM}^{Λ} give the relative orientation of the interaction tensor Λ and a molecule fixed frame with its z-axis along the O^{η}–H^{η} internuclear vector and its x-axis perpendicular to the C^{ζ}–O^{η}–H^{η} plane.[14]

[b] Experimental results.[14]

[c] Results of DFT calculations.[14]

[d] Set, so that the $^{17}\mathrm{O}^{\eta}$ and $^{1}\mathrm{H}^{\eta}$ spectral peaks are on-resonance with the rf carrier frequency.

Table S1: Relevant spin interactions in $^{17}\mathrm{O}^{\eta}$-L-tyrosine·HCl used in the numerically exact spin simulations. The $^{17}\mathrm{O}^{\eta}$–$^{1}\mathrm{H}^{\eta}$ and $^{17}\mathrm{O}^{\eta}\cdots{}^{1}\mathrm{H}''$ dipolar coupling constants were varied during the simulations, where the O^{η}–H^{η} and O''–H'' bond directions were taken from the neutron-diffraction-determined structure[20] and the $^{1}\mathrm{H}^{\eta}\cdots{}^{1}\mathrm{H}''$ dipolar coupling was adjusted accordingly in all cases.[14]

term is only 1–1.5 % of the size of the ^{17}O–^{1}H heteronuclear dipolar coupling.[14]

2.4 Data analysis

The experimental data points shown in Figures 3b, 3d, 3f, and S2 correspond to the normalized experimental integrals of the $^{17}\mathrm{O}^{\eta}$ spectral peak (complete second-order lineshape) plotted as a function of the duration τ of the recoupling pulse sequence. The peak integrals were in all cases normalized to the peak integral at $\tau = 0$.

2.4.1 Non-proton-selective experiments

Figure 3b shows the results obtained with the non-proton-selective scheme in Figure 2a. The solid line corresponds to the best-fit result of numerically exact two-spin ($^{17}\mathrm{O}^{\eta}$, $^{1}\mathrm{H}^{\eta}$) simulations. The numerically simulated ^{17}O signal amplitudes are denoted $a(b_{\mathrm{H}^{\eta}\mathrm{O}^{\eta}}, \tau)$,

where $b_{\mathrm{H}^{\eta}\mathrm{O}^{\eta}}$ is the $^{17}\mathrm{O}^{\eta}$–$^{1}\mathrm{H}^{\eta}$ heteronuclear dipolar coupling constant. All relevant spin-interactions were taken into account and $b_{\mathrm{H}^{\eta}\mathrm{O}^{\eta}}/2\pi$ was varied in steps of 10 Hz from 13500 Hz to 16500 Hz. The amplitudes $a(b_{\mathrm{H}^{\eta}\mathrm{O}^{\eta}}, \tau)$ were multiplied by an exponential damping factor $f \exp\{-\tau/T_R\}$ to take relaxation into account. In addition, an empirical exponentially damped constant offset $(1-f)\exp\{-\tau/T_{\mathrm{qe}}\}$ was added to satisfactorily fit the calculated curves to the experimental signal intensities. This offset is attributed to the complex relaxation pathways in the proton network that leads to a decaying quasi-equilibrium state.[21,22] The resulting fitting function for the experimental $^{17}\mathrm{O}$ signal amplitudes is given by:

$$s(b_{\mathrm{H}^{\eta}\mathrm{O}^{\eta}}, \tau) = a(b_{\mathrm{H}^{\eta}\mathrm{O}^{\eta}}, \tau) f \exp\{-\tau/T_R\} + (1-f)\exp\{-\tau/T_{\mathrm{qe}}\} \tag{S15}$$

We obtained the 95 % confidence interval for the heteronuclear dipolar coupling by calculating the mean squared deviation S between the experimental and simulated amplitudes for the set of heteronuclear dipolar couplings $b_{\mathrm{H}^{\eta}\mathrm{O}^{\eta}}$, where for each value of $b_{\mathrm{H}^{\eta}\mathrm{O}^{\eta}}$ the other 3 fitting parameters $(f, T_R, T_{\mathrm{eq}})$ were optimized as to minimize S. The 95 % confidence interval is determined by the set of dipolar couplings for which $S \leq S_{\min}\{1+F^{0.05}_{1,n-4}/(n-4)\}$, where $S_{\min}$ is the mean squared deviation between experimental and simulated amplitudes minimized by optimizing all 4 fitting parameters and n is the number of experimental points. $F^{\alpha}(p_1, p_2)$ is the upper α probability point of the F distribution with p_1 and p_2 degrees of freedom.[23]

The best fit results for the heteronuclear dipolar $^{17}\mathrm{O}^{\eta}$–$^{1}\mathrm{H}^{\eta}$ coupling constants $b_{\mathrm{O}^{\eta}\mathrm{H}^{\eta}}$, the factor f and the relaxation time constants T_R and T_{qe} are given by $(b_{\mathrm{O}^{\eta}\mathrm{H}^{\eta}}/2\pi, f, T_R, T_{\mathrm{qe}}) = (14770 \pm 260\ \mathrm{Hz}, 0.99, 2.12\ \mathrm{ms}, 45.2\ \mathrm{ms})$. The $^{17}\mathrm{O}^{\eta}$–$^{1}\mathrm{H}^{\eta}$ heteronuclear dipolar coupling constant corresponds to an NMR distance of $r_{\mathrm{NMR}} = 103.3\ (+0.6, -0.5)$ pm. This is about 4.4 % larger than the distance of $r_{n\text{-diff}} = 98.9$ pm estimated by neutron diffraction, which can be attributed to the librational motion of the O^{η}–H^{η} bond vector. It should be noted that the influence of the $^{17}\mathrm{O}^{\eta}\cdots{}^{1}\mathrm{H}''$ heteronuclear dipolar coupling (medium-range intermolecular distance) on the determination of the $^{17}\mathrm{O}^{\eta}$–$^{1}\mathrm{H}^{\eta}$ heteronuclear dipolar cou-

pling (short-range interbond distance) is very small, as has been discussed before in Ref. 14 and which is confirmed by the proton-selective experiments.

The dotted lines in Figure 3b are the result of an average Hamiltonian calculation according to Eq. (15) in Ref. 14 considering solely the heteronuclear dipolar coupling and using the same fitting parameters as for the numerically exact simulations. The agreement with the numerically exact simulations is very good, demonstrating the robustness of the $SR4_1^2$ recoupling sequences with respect to ^{17}O quadrupolar couplings and both ^{17}O and ^1H chemical shift anisotropies. Therefore the analysis of the experimental curves may for simplicity be done just using average Hamiltonian calculations, which are much faster than numerically exact simulations.

2.4.2 Proton-selective experiments

Figures 3d (S2a) and 3f (S2c) show the experimental heteronuclear modulation curves obtained with the proton-selective pulse scheme in Figure 2b, employing Gaussian 180° pulses selective to the $^1H^{\eta}$ and $^1H''$ sites, respectively. In addition, Figures S2b and S2d show the results of control experiments where the Gaussian pulse on the protons was left out. In this case all ^{17}O–^1H heteronuclear dipolar couplings are refocused during the second evolution time under the $SR4_1^2$ sequence.

The solid lines in Figure 3d (S2a) and Figure 3f (S2c) correspond to the best-fit results of numerically exact two-spin ($^{17}O^{\eta}$, $^1H^{\eta}$) and ($^{17}O^{\eta}$, $^1H''$) simulations respectively. The numerically simulated ^{17}O signal amplitudes are denoted $a^{\mathrm{sel}}(b_{IS}, \tau)$, where $(I, S) = \{(H'', O^{\eta}), (H^{\eta}, O^{\eta})\}$ is the spin-pair of interest. In the case of $a^{\mathrm{sel}}(b_{H^{\eta}O^{\eta}}, \tau)$ the heteronuclear dipolar coupling constant $b_{H^{\eta}O^{\eta}}/2\pi$ was varied in steps of 10 Hz from 13500 Hz to 16500 Hz, whereas in the case of $a^{\mathrm{sel}}(b_{H''O^{\eta}}, \tau)$ the heteronuclear dipolar coupling constant $b_{H''O^{\eta}}/2\pi$ was varied in steps of 10 Hz from 2000 Hz to 6000 Hz. The fitting

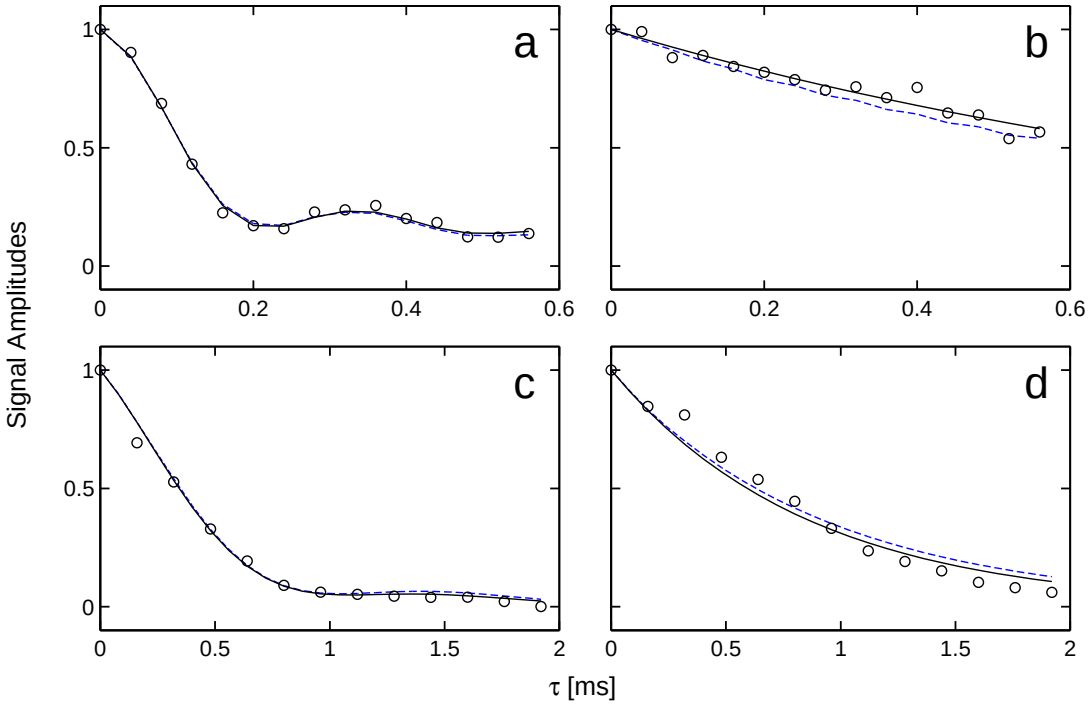

Figure S2: Symbols: Normalized experimental integrals of the $^{17}O^{\eta}$ spectral peak as a function of the duration τ of the $SR4_1^2$ recoupling sequence using the pulse scheme in Figure 2b: (a) employing a $^1H^{\eta}$-selective Gaussian pulse, (b) control experiment to (a) without Gaussian pulse, (c) employing a ^1H"-selective Gaussian pulse, and (d) control experiment to (c) without Gaussian pulse. Solid lines: Best-fit numerical two-spin simulations. Dashed lines: Best-fit numerical three-spin simulations.

functions of the experimental ^{17}O signals amplitudes are given by:

$$s^{\mathrm{sel}}(b_{IS},\tau) = a^{\mathrm{sel}}(b_{IS},\tau) f \exp\{-\tau/T_R\} + (1-f)\exp\{-\tau/T_{\mathrm{qe}}\} \tag{S16}$$

$$s_0^{\mathrm{sel}}(b_{IS},\tau) = f \exp\{-\tau/T_R\} + (1-f)\exp\{-\tau/T_{\mathrm{qe}}\}, \tag{S17}$$

where s^{sel} and s_0^{ssel} are the fitting functions for the experimental heteronuclear modulation curve and the control experiment, respectively. Both the experimental modulation curve and the control experiment were fitted simultaneously in each case. The 95 % confidence intervals for the heteronuclear dipolar couplings were determined as has been described in section 2.4.1 before. In case of the $^1H^{\eta}$-selective experiment, the experimental results in Figure 3d (S2a) and Figure S2b were fitted simultaneously. The best fit results are given by $(b_{O^{\eta}H^{\eta}}/2\pi, f, T_R, T_{\mathrm{qe}}) = (14270\ [+580, -550]\ \mathrm{Hz}, 0.78, 1.01\ \mathrm{ms}, 1.10\ \mathrm{ms})$. The $^{17}O^{\eta}$–

$^1\mathrm{H}^\eta$ heteronuclear dipolar coupling constant corresponds to an NMR distance of $r_{\mathrm{NMR}} = 104.5 \pm 1.4$ pm, which is in agreement within the error margins with the results of the non-proton-selective experiment. In case of the $^1\mathrm{H}''$-selective experiment, the experimental results in Figure 3f (S2c) and Figure S2d were fitted simultaneously. The best fit results are given by $(b_{\mathrm{O}^\eta\mathrm{H}''}/2\pi, f, T_R, T_{\mathrm{qe}}) = (3130\ [+660, -550]\ \mathrm{Hz}, 0.79, 0.88\ \mathrm{ms}, 0.78\ \mathrm{ms})$. The $^{17}\mathrm{O}^\eta$–$^1\mathrm{H}''$ heteronuclear dipolar coupling constant corresponds to an NMR distance of $d_{\mathrm{NMR}} = 173\ (+12, -11)$ pm, which is about 8 % larger than the distance of $d_{n\text{-diff}} = 160.9$ pm estimated by neutron diffraction. The accuracy is satisfactory considering the difficulty of measuring these type of distances by NMR.

Numerical simulations in two- and three-spin systems show that the effect of an imperfect inversion pulse on the protons is to add an offset to the dipolar modulation curves, where the frequency of the dipolar modulation is not effected. Therefore this effect is included in the offset parameter f of the fitting functions.

The dotted lines in Figure 3d and 3f are the result of two-spin average Hamiltonian calculation according to Eq. (15) in Ref. 14 considering solely the relevant heteronuclear dipolar coupling and using the same fitting parameters as for the numerical two-spin simulations. The agreement with the numerically exact simulations is again very good as has been seen before in the case of the non-proton-selective experiments.

The dashed lines in Figure 3d (S2a) and Figure 3f (S2c) correspond to the best-fit results of numerically exact three-spin ($^{17}\mathrm{O}^\eta$, $^1\mathrm{H}^\eta$, $^1\mathrm{H}''$) simulations. The numerically simulated ^{17}O signal amplitudes are denoted $a^{\mathrm{sel}}_{\mathrm{H}^\eta}(b_{\mathrm{O}^\eta\mathrm{H}^\eta}, b_{\mathrm{O}^\eta\mathrm{H}''}, \tau)$ and $a^{\mathrm{sel}}_{\mathrm{H}''}(b_{\mathrm{O}^\eta\mathrm{H}^\eta}, b_{\mathrm{O}^\eta\mathrm{H}''}, \tau)$ for the experiments employing Gaussian 180° pulses selective to the $^1\mathrm{H}^\eta$ and $^1\mathrm{H}''$ sites, respectively. In addition we calculated the the signal amplitudes $a^{\mathrm{sel}}_0(b_{\mathrm{O}^\eta\mathrm{H}^\eta}, b_{\mathrm{O}^\eta\mathrm{H}''}, \tau)$ for the control experiment leaving out the Gaussian pulse on the protons. These numerical simulations show no modulation of the signal amplitudes as expected. The pair of heteronuclear dipolar coupling constants $(b_{\mathrm{O}^\eta\mathrm{H}^\eta}, b_{\mathrm{O}^\eta\mathrm{H}''})$ was varied on a two-dimensional grid, were $b_{\mathrm{O}^\eta\mathrm{H}^\eta}$ was incremented in steps of 100 Hz from 2000 Hz to 5000 Hz and $b_{\mathrm{O}^\eta\mathrm{H}''}$ was incremented in steps of 100 Hz from 13000 Hz to 16000 Hz. The fitting functions of the

experimental ^{17}O signals amplitudes are given by:

$$s^{\mathrm{sel}}_{\mathrm{H}^{\eta}}(b_{\mathrm{O}^{\eta}\mathrm{H}^{\eta}}, b_{\mathrm{O}^{\eta}\mathrm{H}^{\prime\prime}}, \tau) = a^{\mathrm{sel}}_{\mathrm{H}^{\eta}}(b_{\mathrm{O}^{\eta}\mathrm{H}^{\eta}}, b_{\mathrm{O}^{\eta}\mathrm{H}^{\prime\prime}}, \tau) f \exp\{-\tau/T_R\} + (1-f)\exp\{-\tau/T_{\mathrm{qe}}\} \quad \text{(S18)}$$

$$s^{\mathrm{sel}}_{\mathrm{H}^{\prime\prime}}(b_{\mathrm{O}^{\eta}\mathrm{H}^{\eta}}, b_{\mathrm{O}^{\eta}\mathrm{H}^{\prime\prime}}, \tau) = a^{\mathrm{sel}}_{\mathrm{H}^{\prime\prime}}(b_{\mathrm{O}^{\eta}\mathrm{H}^{\eta}}, b_{\mathrm{O}^{\eta}\mathrm{H}^{\prime\prime}}, \tau) f \exp\{-\tau/T_R\} + (1-f)\exp\{-\tau/T_{\mathrm{qe}}\} \quad \text{(S19)}$$

$$s^{\mathrm{sel}}_{0}(b_{\mathrm{O}^{\eta}\mathrm{H}^{\eta}}, b_{\mathrm{O}^{\eta}\mathrm{H}^{\prime\prime}}, \tau) = a^{\mathrm{sel}}_{0}(b_{\mathrm{O}^{\eta}\mathrm{H}^{\eta}}, b_{\mathrm{O}^{\eta}\mathrm{H}^{\prime\prime}}, \tau) f \exp\{-\tau/T_R\} + (1-f)\exp\{-\tau/T_{\mathrm{qe}}\} \quad \text{(S20)}$$

where $s^{\mathrm{sel}}_{\mathrm{H}^{\eta}}$ and $s^{\mathrm{sel}}_{\mathrm{H}^{\prime\prime}}$ are the fitting functions for the experimental heteronuclear modulations curves and s^{sel}_{0} is the fitting functions for the control experiments. All experimental results shown in Figure 3d (S2a), Figure S2b, Figure 3f (S2c) and Figure S2d were fitted simultaneously. The best fit results are given by $(b_{\mathrm{O}^{\eta}\mathrm{H}^{\eta}}/2\pi, b_{\mathrm{O}^{\eta}\mathrm{H}^{\prime\prime}}/2\pi, f, T_R, T_{\mathrm{qe}}) = (14200\ \mathrm{Hz}, 3100\ \mathrm{Hz}, 0.77, 0.98\ \mathrm{ms}, 0.84\ \mathrm{ms})$. It should be noted that in this case the same relaxation constants were used for both the $(\mathrm{O}^{\eta}, \mathrm{H}^{\eta})$ and $(\mathrm{O}^{\eta}, \mathrm{H}^{\prime\prime})$ modulation curves. This is certainly a strong simplification and explains that the fits for the three-spin simulations are slightly worse than for the two-spin simulations. However the result for the heteronuclear dipolar coupling constants is in good agreement between two- and three-spin simulations.

References

1. Lee, Y. K.; Kurur, N. D.; Helmle, M.; Johannessen, O. G.; Nielsen, N. C.; Levitt, M. H. *Chem. Phys. Lett.* **1995,** *242,* 304–309.

2. Edén, M.; Levitt, M. H. *J. Chem. Phys.* **1999,** *111,* 1511–1519.

3. Brinkmann, A.; Edén, M.; Levitt, M. H. *J. Chem. Phys.* **2000,** *112,* 8539–8554.

4. Carravetta, M.; Edén, M.; Zhao, X.; Brinkmann, A.; Levitt, M. H. *Chem. Phys. Lett.* **2000,** *321,* 205–215.

5. Brinkmann, A.; Levitt, M. H. *J. Chem. Phys.* **2001,** *115,* 357–384.

6. Carravetta, M.; Edén, M.; Johannessen, O. G.; Luthman, H.; Verdegem, P. J. E.; Lugtenburg, J.; Sebald, A.; Levitt, M. H. *J. Am. Chem. Soc.* **2001,** *123,* 10628–10638.

7. Levitt, M. H. Symmetry-Based Pulse Sequences in Magic-Angle Spinning Solid-State NMR. In *Encyclopedia of Nuclear Magnetic Resonance*, Vol. 9; Grant, D. M.; Harris, R. K., Eds.; Wiley: Chichester, England, 2002.

8. Brinkmann, A.; Edén, M. *J. Chem. Phys.* **2004,** *120,* 11726–11745.

9. Brinkmann, A.; Schmedt auf der Günne, J.; Levitt, M. H. *J. Magn. Reson.* **2002,** *156,* 79–96.

10. Edén, M. *Chem. Phys. Lett.* **2002,** *366,* 469–476.

11. Kristiansen, P. E.; Carravetta, M.; Lai, W. C.; Levitt, M. H. *Chem. Phys. Lett.* **2004,** *390,* 1–7.

12. Levitt, M. H. Composite Pulses. In *Encyclopedia of Nuclear Magnetic Resonance*, Vol. 2; Grant, D. M.; Harris, R. K., Eds.; Wiley: Chichester, England, 1996.

13. Edén, M. *Chem. Phys. Lett.* **2003,** *378,* 55–64.

14. Brinkmann, A.; Kentgens, A. P. M. *J. Phys. Chem. B* **2006,** *110,* 16089–16101.

15. Samoson, A.; Tuherm, T.; Gan, Z. *Solid State NMR* **2001,** *20,* 130–136.

16. van Beek, J. D. MatNMR is a toolbox for processing NMR/EPR data under MATLAB and can be freely downloaded at http://matnmr.sourceforge.net.

17. Levitt, M. H. *J. Magn. Reson.* **1997,** *126,* 164–182.

18. Bak, M.; Nielsen, N. C. *J. Magn. Reson.* **2000,** *147,* 296–330.

19. Cheng, V. B.; Henry H. Suzukawa, J.; Wolfsberg, M. *J. Chem. Phys.* **1973,** *59,* 3992–3999.

20. Frey, M. N.; Koetzle, T. F.; Lehmann, M. S.; Hamilton, W. C. *J. Chem. Phys.* **1973,** *58,* 2547–2556.

21. Sakellariou, D.; Hodgkinson, P.; Emsley, L. *Chem. Phys. Lett.* **1998,** *293,* 110–118.

22. Williamson, P. T. F.; Verhoeven, A.; Ernst, M.; Meier, B. H. *J. Am. Chem. Soc.* **2003,** *125,* 2718–2722.

23. Seber, G. A. F.; Wild, C. J. *Nonlinear Regression;* Wiley Series in Probability and Statistics Wiley-Interscience: Hoboken, USA, 2003.